

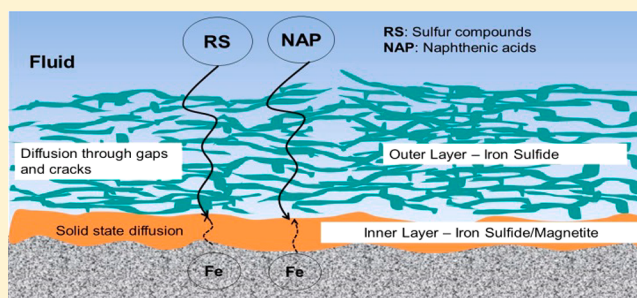
High-Temperature Corrosion by Carboxylic Acids and Sulfidation under Refinery Conditions—Mechanism, Model, and Simulation

Peng Jin,^{*,} Winston Robbins, and Gheorghe Bota

Department of Chemical and Biomolecular Engineering, Ohio University, 342 West State Street, Athens, Ohio 45701, United States

S Supporting Information

ABSTRACT: In crude oil refineries, high temperature corrosion in nonaqueous phase, predominantly by carboxylic acids (also known as naphthenic acids in crude oil) and sulfidation, is an old problem and has been studied for almost a century. Despite the large body of laboratory study and field experience, the mechanism of corrosion by naphthenic acids and sulfidation is not fully understood so that models in the public domain are empirical rather than mechanistic. Previously, a protective inner iron oxide scale was found when both naphthenic acids and sulfur compounds were present in our prior corrosion study. In the current study, it is shown that the high-temperature corrosion by naphthenic acids and sulfidation depends on the solid state diffusion of iron through the inner scale. It is postulated that corrosion rates are governed by either chemical kinetics on the surface of the inner scale or self-diffusion of iron through the inner scale. A model was built to simulate this mechanism for corrosion and validated with experimental data from a flow through corrosion test.



1. INTRODUCTION

In recent years, there was an increasing economic stimulus for crude oil refineries to process price-discounted “opportunity crudes”. It is estimated that processing opportunity crudes may boost the profit of a medium-sized refinery by more than ten million US dollars (USD) each year.¹ However, the high content of sulfur compounds and carboxylic acids (also known as naphthenic acids in the crude oil, NAP) may cause serious corrosion problems and threaten facility integrity.

Although sulfidation (corrosion by sulfur compounds in the crude oil) and naphthenic acid corrosion (NAC) have been studied for decades,² most studies are empirical, describing experimental results and field experience without probing the corrosion mechanism. For example, sulfidation is often predicted by modified McConomy curves that relate corrosion rates with temperature for different alloys based on refinery experience data with an implication of mechanism. Total sulfur is used for correlations, although functional groups (mercaptan, aliphatic/alicyclic sulfide, disulfide, thiophene) differ in abundance and reactivity.^{3–6} Large numbers of NAP with different structures are present in acidic crude oils.^{7–11} Corrosion by NAC is generalized leaving no solid corrosion product on the steel surface after undermining thin oxide layer steel surfaces.¹²

Despite extensive study, the mechanism of concurrent sulfidation and NAC is still not understood on a molecular level. Publications on “corrosion models” describe generic observations on sulfidation and NAC or proprietary empirical correlations between the corrosion rate and the corrosive

environment.^{1,13–15} Currently, there is no public mechanistic model to simulate sulfidation and NAC.

1.1. Background. In our prior research into the mechanism, a multilayer corrosion product scale was found to have an inner oxygen-containing layer underneath an outer sulfide layer after the concurrent sulfidation and NAC.^{16,17} The inner layer (inner scale) was found to be a mixture of nanoparticulate magnetite and pyrrhotite while the outer layer (outer scale) was composed of pyrrhotite only. It was determined that the presence of magnetite in the inner scale significantly enhanced the layer protectiveness.^{18–20} The formation of magnetite in the inner scale was rationalized to be the result of thermal decomposition of iron naphthenates (iron carboxylates) formed by acid attack on the metal followed by the disproportionation of wüstite (FeO) trapped underneath the outer scale (reactions R1 and R2).^{21–25}



In the current study, it is proposed that the sulfidation and NAC by crude oil is controlled by the solid state diffusion of iron through the inner corrosion product scale adjacent to the steel surface. A model has been built on the basis of the proposed corrosion mechanism. The mechanistic model has

Received: January 17, 2018

Revised: March 5, 2018

Accepted: March 7, 2018

Published: March 7, 2018

been validated by simulation of a series of experiments involving solutions of various acid concentrations (denoted by TAN or total acid number, the amount of potassium hydroxide in milligram to naturalize one gram crude oil) and sulfur content. To the best knowledge of the authors, it is the first mathematical model based on the corrosion mechanism of sulfidation and NAC in the public domain.

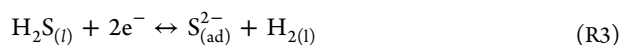
1.2. Corrosion Mechanism. In contrast to the electrochemical reactions in aqueous corrosion, sulfidation, and NAC are generally accepted to proceed by direct chemical reactions due to the range of 10^{10} – 10^{15} $\Omega\cdot\text{m}$ resistivity of crude oils.^{26,27} One of challenges in studying corrosion mechanisms is the formation and growth of corrosion product scale. For example, a dense scale composed of iron sulfide and/or iron carbonate is found in aqueous corrosion with carbon dioxide (CO_2) and/or hydrogen sulfide (H_2S). It is commonly accepted that the dense scale deters the aqueous diffusion of corrosive ions and $\text{CO}_2/\text{H}_2\text{S}$ toward the steel surface and decreases the corrosion rate.^{28–34} While the thickness of an outer FeS layer may affect molecular diffusion toward the surface in a similar fashion, the role of the inner scale in sulfidation and NAC is less clear. Two hypotheses may be proposed for its effect on corrosion:

Hypothesis 1: The porosity of the inner scale allows corrosive molecular species in the fluid to diffuse toward the steel surface so that the corrosion reaction takes place at the steel surface under the corrosion product scale.

Hypothesis 2: The inner scale is impermeable to molecular species in the fluid but allows solid state diffusion of iron through it so that corrosion takes place on the outer surface of the inner scale.

Hypothesis 1 is an intuitive extension of the role of scale in aqueous corrosion that replaces ions in an electrolyte at temperatures below 200 °C with direct reaction of reactive sulfur and acid molecules in a nonconducting medium at temperatures above 200 °C. At these temperatures below 200 °C solid state diffusion is usually ignored.

Hypothesis 2 is an intuitive extension of oxidation and sulfidation at temperatures well above 400 °C where solid state diffusion of iron through an inner scale is fast.³⁵ Radiotracer and magnetokinetic measurements over the past 70 years has established that the high-temperature sulfidation of steel proceeds by the outward diffusion of iron through the compact iron sulfide scale by exchange between an iron atom and the neighboring vacancy.^{36–43} Gas phase sulfidation has been proven to proceed by charge transfer with incorporation of sulfur atoms into the iron sulfide lattice and creation of charged iron vacancies (reactions R3–R6).^{44–46} Continuous sulfidation results in an iron-deficient outer surface of the inner scale and promotes the solid state diffusion of iron.



High temperature solid state diffusion studies involve gas phase concentrations (i.e., very low concentrations) of reactive molecules in inert carrier gases with no mechanism for scale removal. In less inert refinery liquids at 240–400 °C, iron solid state diffusion and chemical reaction rates for sulfidation and NAC are similar in order of magnitude but the complex liquids

can remove corrosion products by shear stress or solubility forces.

Under refinery conditions sulfidation and NAC usually proceed simultaneously. In our prior study, scales formed on specimens by sulfidation and NAC are challenged by an acid only flow at TAN 3.5.^{16,17} When the experiment was performed in a flow through mini-autoclave (FTMA), oxygen in the inner scale was observed to enhance the scale protectiveness when challenged by acids alone.^{47,48} The composition, location, and thickness of the scales in this study were taken as evidence that solid state diffusion of iron was the controlling mechanism, i.e. concurrent NAC and sulfidation by model compounds generated an impermeable inner scale. As a corollary, magnetite in an inner scale is expected to reduce corrosion rates because its solid state diffusivity is several orders lower than that in pyrrhotite (Figure 1).⁴³ The results of the experiments in following sections reinforce the conclusion that hypothesis 2 is correct.

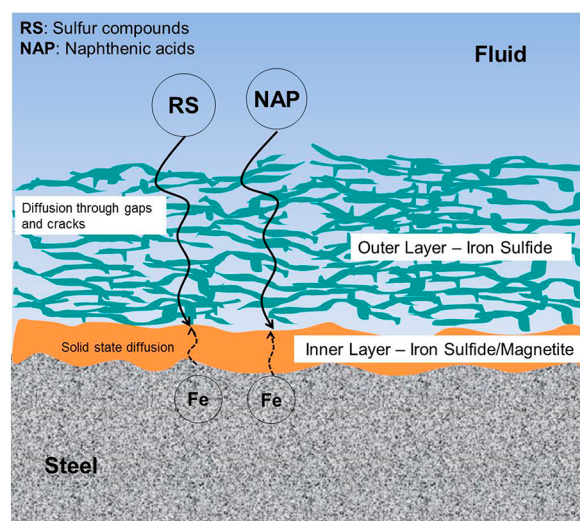


Figure 1. Solid state diffusion of iron through the inner scale.

2. MODELING APPROACH

The model assumes that corrosion is governed by two processes—the solid state diffusion of iron through the inner scale and the chemical reactions on the surface of the inner scale—either of which may be rate-determining. In addition, it assumes that molecular diffusion in the fluid and flow dynamics influence rates of chemical reactions by affecting the concentration of NAP and sulfur compounds at the surface of the inner scale. Each factor is addressed below.

2.1. Solid State Diffusion of Iron. As noted above, the solid state diffusion of iron in iron sulfide proceeds by the exchange between ferrous ions (Fe^{2+}) and the vacancies in the lattice. Previously, XRD identified troilite as the form of FeS in the corrosion product scale; however, other work shows that the FeS is more properly identified as a pyrrhotite ($\text{Fe}_{(1-x)}\text{S}$) that is indistinguishable from troilite in XRD.⁴⁹ The iron diffusivity in pyrrhotite may be calculated by eq 1.³⁹ In the current study, the adopted value of diffusion activation energy ($\Delta H_{\text{Fe in FeS}}$) is 82 kJ/mol when temperature is above the Néel temperature of pyrrhotite (316 °C).⁴² It is known that the pre-exponential factor $D_{0,\text{Fe in FeS}}$ is a function of crystal orientation with the average value 2×10^{-6} m^2/s for random orientation as

Table 1. Chemical Composition of A106 Carbon Steel Specimen (% wt)

C	Si	Mn	P	S	Cr	Ni	Mo	V	Cu	Fe
0.18	0.41	0.8	0.11	0.06	0.02	0.04	0.02	0.03	0.08	bal

expected for the inner scale.³⁹ The pre-exponential factor for iron in magnetite $D_{0,Fe \text{ in } Fe_3O_4}$ with random orientation is the same order of magnetite ($0.5\text{--}5 \times 10^{-6} \text{ m}^2/\text{s}$).⁵⁰ However, when iron diffusion in magnetite is calculated by eq 2 with its diffusion activation energy ($\Delta H_{Fe \text{ in } Fe_3O_4}$) of 240 kJ/mol, it can be seen that there is a high energy barrier for the motion of iron that explains its superior corrosion protectiveness.⁴³

$$D_{Fe \text{ in } FeS} = D_{0,Fe \text{ in } FeS} e^{-\Delta H_{Fe \text{ in } FeS}/RT} \quad (1)$$

$$D_{Fe \text{ in } Fe_3O_4} = D_{0,Fe \text{ in } Fe_3O_4} e^{-\Delta H_{Fe \text{ in } Fe_3O_4}/RT} \quad (2)$$

For the inner scale composed of compact nonporous nanoparticulate pyrrhotite and magnetite, the effective diffusivity can be found by the Maxwell equation as shown below.³⁵

$$D_{eff} = \frac{D_{Fe \text{ in } FeS}[(3 - 2V_{FeS})D_{Fe \text{ in } Fe_3O_4} + 2V_{FeS}D_{Fe \text{ in } FeS}]}{V_{FeS}D_{Fe \text{ in } Fe_3O_4} + (3 - V_{FeS})D_{Fe \text{ in } FeS}} \quad (3)$$

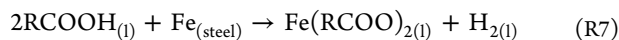
In the steady state, the diffusion rate of iron through the inner scale is proportional to the concentration gradient of iron according to the Fick's law (eq 4).

$$J_{Fe} = \frac{D_{eff}}{\delta} (C_{0,Fe} - C_{i,Fe}) \quad (4)$$

When there are sufficient quantities of sulfur compounds in the fluid, the incorporation of sulfur atoms proceeds so fast that $C_{i,Fe}$ was zero. In this case, the maximum flux of iron is achieved and the corrosion is limited by the solid state diffusion of iron (eq 5).

$$J_{Fe,max} = \frac{D_{eff}}{\delta} C_{0,Fe} \quad (5)$$

2.2. Chemical Reactions in Corrosion. In the absence of corrosion product scale, NAP corrodes the steel directly (reaction R7). Note that both reaction products can be continuously removed from the steel surface so that the reverse reaction is often ignored. NAC has been shown to be a first-order reaction regarding NAP, and the corrosion rate follows the Arrhenius law (eq 6).^{51,52}



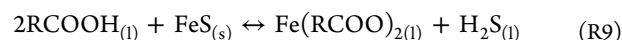
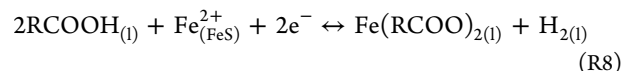
$$r_{NAC \text{ on } steel} = C_{s,NAP} A_{NAC \text{ on } steel} e^{-\Delta H_{NAC \text{ on } steel}/RT} \quad (6)$$

The rate-determining step (RDS) of sulfidation has been shown to be sulfur exchange (reaction R3), which is a first-order reaction regarding H_2S concentration.⁴⁶ Therefore, the model postulates that sulfidation in the liquid phase is also a first-order reaction determined by eq 7.

$$r_{sulfidation} = C_{s,sulfur} A_{sulfidation} e^{-\Delta H_{sulfidation}/RT} \quad (7)$$

The model assumes that NAC takes place on the surface in the inner scale, i.e. it postulates that NAP reacts with the iron in the of the pyrrhotite lattice (reaction R8). The rate of reaction R8 is assumed to be close to that of reaction R9 which represents the dissolution of pyrrhotite by acids. In both

reactions, the ferrous ion leaves the pyrrhotite lattice and associates with the RCOO group. The difference relates to the byproduct—hydrogen atoms combining with each other to form hydrogen gas in reaction R8 while they associate with sulfur atoms to form hydrogen sulfide in reaction R9.



However, most studies on NAC assume direct corrosion of steel by NAP (reaction R7) rather than by acid attack on the pyrrhotite in the inner scale (reactions R8 and R9). If the model postulates that dissolution of the pyrrhotite by the acids is a first-order reaction, the acid corrosion rate can be calculated by eq 8.

$$r_{NAC \text{ on } FeS} = C_{s,NAP} A_{NAC \text{ on } FeS} e^{-\Delta H_{NAC \text{ on } FeS}/RT} \quad (8)$$

However, no values have been published for the kinetic constants of the high-temperature dissolution of pyrrhotite by carboxylic acids in nonaqueous phase (reaction R9).

For NAC only on bare steel surface, no inner scale is formed and the corrosion rate is calculated by eq 6. In all other cases, an inner scale is formed and the combination of NAC and sulfidation rates is calculated from eqs 7 and 8. In parallel, the maximum solid state diffusion of iron is calculated from eq 5. The corrosion rate is from the rate limiting step, i.e. either the value of the chemical reaction rate or the maximum solid state diffusion of iron (eq 9).

$$CR_{simulation} = \text{minimum}\{(r_{NAC \text{ on } FeS} + r_{sulfidation}), J_{Fe,max}\} \quad (9)$$

The following experimental sections describe the methods to find or estimate the activation energies and pre-exponential terms for eqs 6–8 that are used in the model. In addition, results from a series of experiments that support the corrosion mechanism and model are presented.

3. EXPERIMENTAL SECTION

3.1. Experiment Materials. Rectangular A106 carbon steel (CS) specimens were used in experiments (Table 1, as provided by Alabama Specialty Products). Specimens were 0.60 mm in thickness cut to 16.30 mm × 15.60 mm with a central hole 3.74 mm in diameter. Immediately prior to use, specimens were abraded by 400-grit and 600-grit SiC paper in succession under the flow of 2-propanol, wiped with paper towel to remove residual particles, degreased with toluene and acetone, dried under nitrogen, and weighed with an analytical balance (to obtain an initial weight).

After corrosion experiments, specimens were extracted from the apparatus for weight loss and microscopic analyses. Specimens for weight loss analysis were rinsed with toluene and acetone, prior to Clarke treatment in accordance with ASTM G1-03.^{53,54} Specimens for microscopic analysis were stored in an inert mineral oil until they were rinsed with toluene and acetone just prior to mounting in epoxy for microscopic analysis as described in our previous publication.⁴⁸

Scanning electron microscopy (SEM) analysis was performed on a JEOL JSM-6390 SEM. The energy dispersive X-ray spectroscopy (EDS) detector was equipped with the SEM to analyze the chemical composition.

3.2. Experimental Solutions. The corrosion study was performed with model compounds to represent corrosive NAP and sulfur compounds in real crude oil. *n*-Dodecyl sulfide (DDS, $\text{CH}_3(\text{CH}_2)_{11}\text{S}(\text{CH}_2)_{11}\text{CH}_3$, CAS No. 2469-45-6, Fisher Chemical) was obtained as the model sulfur compound. Model NAP included a mixture of NAP extracted from real crude fractions (TCI, CAS No. 1338-24-5, TCI America, Table 2)

Table 2. Boiling Point Range of TCI (TAN 230)

parameter	temperature (°C)
initial boiling point	239
50% boiling point	296
80% boiling point	343
final boiling point	493

and a pure carboxylic acid—palmitic acid (PA, $\text{CH}_3(\text{CH}_2)_{14}\text{COOH}$, CAS No. 57-10-3, Fisher Chemical). The hydrocarbon of crude oil was replaced by an inert mineral oil Tufflo 6000 by CITGO (Table 3). A series of solutions with different S/TAN ratios were prepared by mixing Tufflo and model compounds (DDS, PA, and TCI) as shown in Table 4.

Table 3. Selected Physical and Chemical Properties—Tufflo

parameter	description
appearance	clear liquid
color	colorless
odor	odorless
density (at 16 °C, kg/m ³)	876
dynamic viscosity (at 100 °C, cP)	1.1
flash point (°C)	254
initial boiling point (°C)	388

Table 4. Properties of Experimental Solutions

solution	TAN	sulfur content (S % wt)	sulfur content/TAN (S/TAN)
PA only	1.75	0	0
PA + DDS-1	1.75	0.25	0.14
PA + DDS-2	1.75	0.58	0.33
PA + DDS-3	1.75	1.16	0.67
PA + DDS-4	1.75	1.75	1
PA + DDS-5	0.87	1.16	1.33
PA + DDS-6	0.87	1.46	1.67
TCI only	3.5	0	0
TCI + DDS	1.75	0.25	0.14
DDS only	0	0.25	-

3.3. Experimental Equipment. A flow through apparatus named “flow through mini autoclave (FTMA)” was used in the experiments. As shown in Figure 2, FTMA allowed continuous fluid fed into its reactor where specimens are installed. In order to avoid cross-contamination, a vessel and an oil pump are devoted to Tufflo only while the other two vessels and oil pump were used to contain and deliver experimental solutions. The fluid fed into the reactor is chosen by switching a three-way valve in the upstream of tubing. During experiments, fluid in all vessels is bubbled with nitrogen gas to remove oxygen. Six specimens separated by spacers are installed in the reactor with

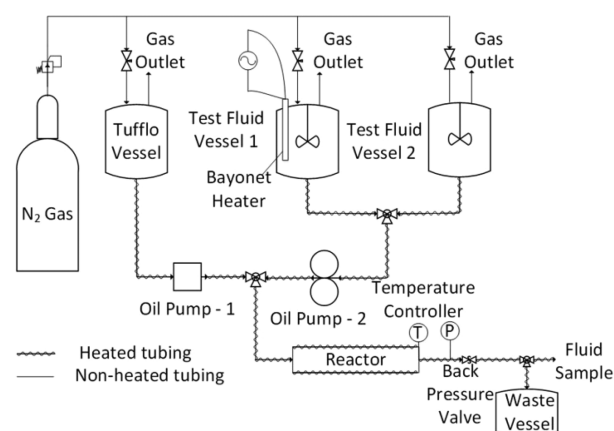


Figure 2. Scheme of the flow through mini autoclave (FTMA).

a thermocouple extended into same location in the reactor to control the temperature of the fluid surrounding the specimens. Details of the specimens installation in the FTMA reactor can be found in our prior publication.⁴⁷ The pressure of reactor (791 kPa) is maintained by the back pressure valve in its downstream. All tubing of FTMA is made of 316 stainless steel, and the customized reactor is made of Hastelloy C-276. The FTMA for the experiments was operated under the conditions shown in Table 5.

Table 5. Flow Parameters of the FTMA Reactor

parameter	value
fluid velocity	9.0×10^{-5} m/s
flow rate	1.5 cm ³ /min
back pressure	791 kPa

3.4. Experimental Procedures. There are two successive steps in an experiments designated as “pretreatment” and “challenge”. The pretreatment experiment is used to generate corrosion product scales in experimental solutions and to assess their corrosivity. In the challenge experiment, the corrosion product scale formed in the pretreatment experiment is exposed to a TAN 3.5 NAP solution at 343 °C for 24 h order to evaluate its protectiveness against NAC. Both steps are run in the FTMA using the experimental procedures described below.

Pretreatment. After installation of freshly abraded specimens, the reactor is connected to the FTMA tubing and a flow of Tufflo is established while when the reactor is being heated to the test temperature. When the test temperature is reached, the flow is switched to the experimental solution contained in test fluid vessel 1 at a flow rate of 1.5 cm³/min. The valve switch is taken as the start of pretreatment experiment. After 24 h, the flow is switched back to Tufflo to remove the residual experimental solution, reactor heating is stopped, and the reactor is allowed to cool down with the Tufflo flow continuing. After cooling, the reactor is opened and drained and the six specimens are removed from the reactor, Three specimens are prepared for weight loss analysis, and the other three are saved in Tufflo for microscopic analysis.

Challenge. A parallel pretreatment experiment is run under the same conditions as described above. In the end of pretreatment time, the valve is switched to Tufflo flowing through the reactor for 30 min while the temperature is adjusted (if necessary) to the challenge temperature 343 °C.

After 30 min (or until 343 °C is reached), the flow is switched to the TAN 3.5 acid solution (“TCI only”) contained in test fluid vessel 2 (1.5 cm³/min). The time of the valve switch is taken as the start of the challenge experiment. After 24 h, the valve is switched back to Tufflo in the end of the challenge. The reactor is cooled down, and specimens are extracted and prepared for analyses in the same manner as in the pretreatment. Thus, in contrast to previous study, the specimens in the FTMA are pretreated and challenged *in situ* without being relocated or subjected to large temperature differences.

3.5. Evaluation of Corrosion Rates. Corrosion rates were calculated by weight loss analysis. Equation 10 shows the expression for the pretreatment corrosion rate. The calculation for the challenge corrosion rate should exclude the weight loss in the pretreatment, as shown in eq 11.

$$CR_1 = \frac{3.15 \times 10^{10} \Delta W_1}{\rho_{\text{steel}} S t} \quad (10)$$

$$CR_2 = \frac{3.15 \times 10^{10} (\Delta W_1 - \Delta W_2)}{\rho_{\text{steel}} S t} \quad (11)$$

4. RESULTS AND DISCUSSION

4.1. Verification of Corrosion Mechanism. Earlier, it was proposed the NAC took place on the outer surface of the inner scale (hypothesis 2). In order to verify the proposed corrosion mechanism, specimens pretreated in FTMA with PA + DDS-5 and -6 solutions at 343 °C were challenged with the TCI only (TAN 3.5) solution in the same FTMA. These experiments at high S/TAN were an extension of our previous work on the effect of S on FTMA scale formation involving PA + DDS-1 to 4. At the high S/TAN ratios, thick inner scales adjacent to steel surface were formed after the pretreatment with PA + DDS-5 and -6 solutions (Figure 3a and c). In the challenge experiment, the corrosion product scale was exposed to the solution containing only NAP, providing valuable information on the mechanism of NAC in the presence of an inner sulfide scale.

The challenge corrosion rates in Table 6 corresponded to a loss in steel thickness of around 4 μm in both cases. In other words, the frontier of the steel surface was expected to “retreat”

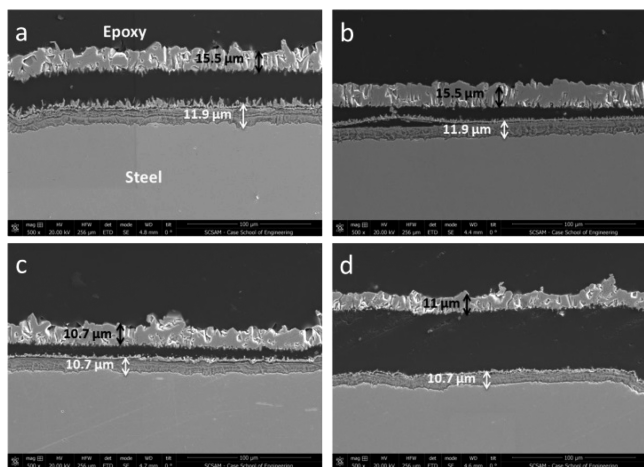


Figure 3. Cross-section SEM images of A106 specimens pretreated in FTMA with PA + DDS-5 (a) and challenged with TCI only (b); pretreated with PA + DDS-6 (c) and challenged with TCI only (d).

Table 6. Pretreatment and Challenge Corrosion Rates of A106 Specimens in PA + DDS-5 and -6 Solutions

pretreatment solution	pretreatment corrosion rate (mm/y)	challenge corrosion rate (mm/y)	steel loss in challenge experiment (μm)
PA + DDS-5	2.6	1.5	4.1
PA + DDS-6	2.8	1.4	3.8

by about 4 μm during the challenge experiment. However, inner layers were intact and still adherent to the steel surface as shown in Figure 3b and d. The fact that the inner layer was not undermined by the acid strongly supported hypothesis 2, i.e. NAC in the presence of inner scale proceeded by the solid state diffusion of iron.

4.2. Determination of Activation Energies of NAC and Sulfidation. The activation energy of NAC on bare steel surface was obtained from the Arrhenius equation based on pretreatment of A106 specimens at different temperatures in the FTMA. As shown in Figure 4, the corrosion rate increases

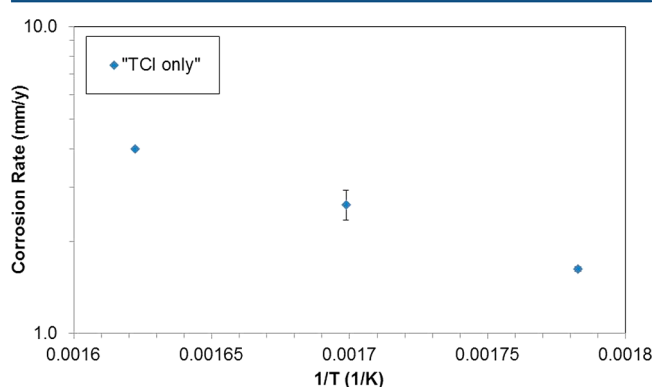


Figure 4. Corrosion rates of A106 specimens pretreated with the TCI only solution in FTMA at 288, 316, and 343 °C.

with temperature and the activation energy ($\Delta H_{\text{NAC on steel}}$ in eq 6) was 47 kJ/mol, which was consistent with reported values in literature.^{52–56} However, the extrapolation of the Arrhenius plot to obtain a pre-exponential factor only yields the product $C_{s,\text{NAP}} A_{\text{NAC on steel}}$ because the concentration of acid at the surface on the inner scale was unknown. In order to calculate the value of the pre-exponential factor $A_{\text{NAC on steel}}$, the NAP concentration on the surface of inner scale ($C_{s,\text{NAP}}$) must be estimated from mass transfer through the fluid and outer scale (read on).

In the same way, A106 specimens were pretreated with a low concentration of DDS only solution (0.25% S) at different temperatures (Figure 5) and the activation energy of sulfidation was found by Arrhenius treatment to be 94 kJ/mol ($\Delta H_{\text{sulfidation}}$ in eq 7). This value was consistent with the activation energy of sulfur (in the form of hydrogen sulfide) exchange on pyrrhotite surface (82–120 kJ/mol).⁵⁷

In order to find the activation energy of reaction R9, A106 specimens pretreated in the DDS only solution were challenged with the TCI only solution. As shown in Figure 6, the inner scale formed in DDS only was partially dissolved after the corrosion by NAP in the challenge experiment and the reaction rate ($r_{\text{NAC on FeS}}$ in eq 8) can be calculated on the basis of thickness decrease (eq 12). Given that the reaction rate was more sensitive to the activation energy than the pre-exponential term, the activation energy of NAC on the pyrrhotite surface

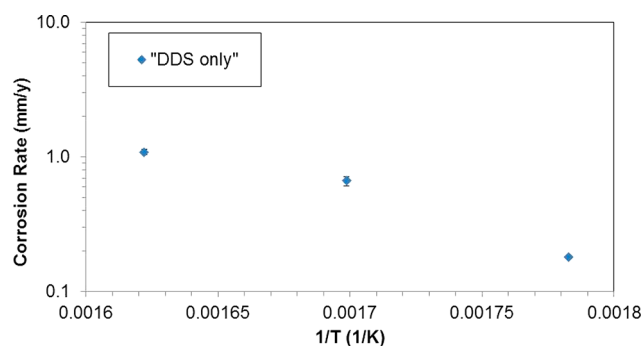


Figure 5. Corrosion rates of A106 specimens pretreated with a 0.25% S DDS only solution in FTMA at 288, 316, and 343 °C.

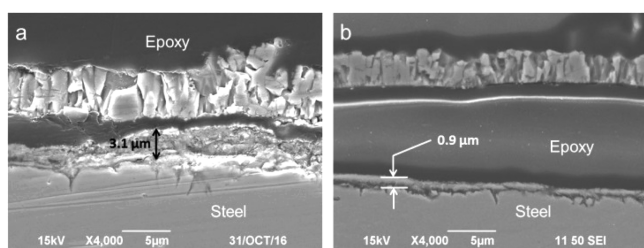


Figure 6. Cross-sectional SEM images of A106 specimens pretreated in FTMA with DDS only at 343 °C (a) and challenged with TCI only (b).

($\Delta H_{\text{NAC on FeS}}$) can be obtained via eq 13, and its value was found to be around 63 kJ/mol.

$$r_{\text{NAC on FeS}} = \frac{\Delta \delta \rho_{\text{FeS}}}{MW_{\text{FeS}} t} \quad (12)$$

$$\frac{r_{\text{NAC on FeS}}}{r_{\text{NAC on steel}}} \approx e^{\Delta H_{\text{NAC on steel}} - \Delta H_{\text{NAC on FeS}} / RT} \quad (13)$$

A summary of activation energies in solid state diffusion and chemical reactions is given in Table 7. This data shows that

Table 7. Activation Energies in Solid State Diffusion and Chemical Reactions

process	activation energy (ΔH , kJ/mol)
self-diffusion of iron in troilite	82
self-diffusion of iron in magnetite	240
$2\text{RCOOH}_{(l)} + \text{Fe}_{(\text{steel})} \leftrightarrow \text{Fe}(\text{RCOO})_{2(l)} + \text{H}_{2(l)}$	47
$\text{H}_2\text{S}_{(l)} + \text{Fe}_{(\text{FeS})} \leftrightarrow \text{FeS}_{(s)} + \text{H}_{2(l)}$	94
$2\text{RCOOH}_{(l)} + \text{FeS}_{(s)} \leftrightarrow \text{Fe}(\text{RCOO})_{2(l)} + \text{H}_2\text{S}_{(l)}$	63

solid state diffusion in magnetite presents the highest energy barrier among all processes, which is consistent with the protectiveness of oxygen-containing scales found in our prior research.^{16–19}

4.3. Mass Transfer in Fluid and Values of Pre-exponential Terms of NAC and Sulfidation. High-temperature diffusion coefficients of NAP and sulfur compounds in oil were not well studied in public literature. C20 paraffin ($\text{C}_{20}\text{H}_{42}$) possesses similar carbon number and molecular size to PA, TCI, and DDS in the current study. Therefore, the self-diffusion of C20 paraffin will be used in the simulation relating to mass transfer in fluid.

The self-diffusion of paraffin has been extensively studied and the diffusion coefficient was fitted in accordance with Eyring's theory (eq 14).^{58–60} For C20 paraffin, $D_{0,\text{C20}}$ was 1.5×10^{-7} m^2/s and ΔH_{C20} , 18 kJ/mol. It was assumed that both NAP and sulfur compounds have the same diffusivity as that of C20 paraffin.

$$D_{\text{C20}} = D_{0,\text{C20}} e^{-\Delta H_{\text{C20}}/RT} \quad (14)$$

In the temperature range of NAC and sulfidation, the dynamic viscosity of C20 paraffin shows a nearly linear relationship with temperature (Figure 7).⁶¹ Although C20 paraffin is a viscous fluid at room temperature, its viscosity at high temperatures is quite low.

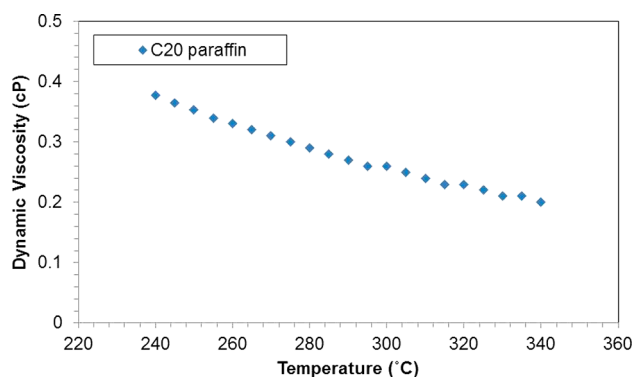


Figure 7. Dynamic viscosity of $\text{C}_{20}\text{H}_{42}$ paraffin at high temperatures. Data obtained from ref 61.

The mass transfer toward the surface of specimens in the FTMA reactor can be solved as a fully developed laminar flow over a horizontal flat plate. The Reynolds number (Re), the Schmidt number (Sc), and the average Sherwood number (Sh) over the plate can be obtained from eqs 15–17.⁶²

$$Re = \frac{lV\rho_{\text{C20}}}{\mu} \quad (15)$$

$$Sc = \frac{\mu}{\rho_{\text{C20}} D_{\text{C20}}} \quad (16)$$

$$Sh = \frac{lk}{D_{\text{C20}}} = 0.664Re^{1/2} Sc^{1/3} \quad (17)$$

Rearrangement of eq 17 gave the mass transfer coefficient (k) in eq 18.

$$k = \frac{0.664Re^{1/2} Sc^{1/3} D_{\text{C20}}}{l} \quad (18)$$

In the steady state, the flux of NAP (J_{NAP}) or sulfur compounds (J_{S}) toward the steel should be equal to their consumption rate in corrosion. According to reaction R7, the consumption rate of NAP is twice that of the corrosion rate of iron, i.e. $J_{\text{NAP}} = 2r_{\text{NAC}}$. For NAC on the bare steel surface, the corrosion rate where no scale is formed is given by eq 6 so that consumption rate of NAP can be calculated by eq 19.

$$\begin{aligned} J_{\text{NAP}} &= k(C_{\text{b,NAP}} - C_{\text{s,NAP}}) \\ &= 2C_{\text{s,NAP}} A_{\text{NAC on steel}} e^{-\Delta H_{\text{NAC on steel}}/RT} \end{aligned} \quad (19)$$

Table 8. Summary of Experimental Conditions to Validate the Model

pretreatment			followed by challenge	description
TAN (mg KOH/g oil)	sulfur content in solution (% wt)	temperature (°C)		
0–1.75	0–1.75%	343	no	corrosion by a series of solutions; data presented in Figure 8
0–1.75	0–1.75%	343	yes	investigation of scale protectiveness; data presented in Figure 9
1.75	0.25%, 0.58%	288–343	no	corrosion at different temperatures; data presented in Figures 10 and 11

From the corrosion rates in Figure 4, the value of pre-exponential term for NAC on bare steel surface ($A_{\text{NAC on steel}}$) was found to be 5.3×10^{-3} m/s.

Extensive studies of have demonstrated that sulfidation quickly reaches a steady state corrosion rate despite increasing scale thicknesses.⁵¹ Because solid state diffusion occurs only through a contiguous inner FeS scale, scale grains separated by mechanical stress no longer participate in reactions with the iron. As noted earlier, the model assumes that sulfidation occurs with a rate limiting sulfur exchange mechanism on the inner scale. The sulfur flux (consumption rate) is equal to the sulfidation rate. Thus, a pre-exponential term of 7.6 m/s for sulfidation ($A_{\text{sulfidation}}$) was calculated from corrosion rates for DDS (eq 20).

$$J_{\text{sulfur}} = k(C_{\text{b,sulfur}} - C_{\text{s,sulfur}}) = C_{\text{s,sulfur}} A_{\text{sulfidation}} e^{-\Delta H_{\text{sulfidation}}/RT} \quad (20)$$

$A_{\text{sulfidation}}$ is 3 orders of magnitude higher than A_{NAP} because the probability that two acid molecules “collide” with a single iron atom is that much lower than the single collision of a reactive sulfur molecule with an iron atom.

4.4. Model Validation with Experimental Results. In order to verify the proposed corrosion mechanism and model, a series of experiments was performed and summarized in Table 8. The thickness and chemical composition of inner scales were determined by analysis of cross-section SEM/EDS of specimens pretreated with a series of PA + DDS in FTMA at 343 °C (Table S1).⁴⁷ No inner scale was formed in the FTMA pretreatment with PA only; otherwise, the thickness and sulfur content of inner scale increased with sulfur content in the solution, indicating sulfidation became the dominant corrosion mechanism for high-sulfur solutions. Assuming the inner scale was a compact mixture of nanoparticulate pyrrhotite and magnetite with no porosity, the volume fraction of iron sulfide was obtained in eq 21, providing the input value to calculate the effective diffusivity in eq 3.

$$V_{\text{FeS}} = \frac{\frac{\text{FeS \% at } MW_{\text{FeS}}}{\rho_{\text{FeS}}}}{\frac{\text{FeS \% at } MW_{\text{FeS}}}{\rho_{\text{FeS}}} + \frac{(1 - \text{FeS \% at}) MW_{\text{Fe}_3\text{O}_4}}{\rho_{\text{Fe}_3\text{O}_4}}} \quad (21)$$

With the thickness of scale and its volume fraction of FeS in Table S1 the solid state diffusivity of iron can be calculated to determine the maximum flux of iron $J_{\text{Fe,max}}$ in eq 5. The simulation (eq 9) calculates the minimum between chemical reaction rate, i.e. the sum of sulfidation and NAC (eqs 7 and 8) and $J_{\text{Fe,max}}$ the solid state limiting rate (eq 5). The values calculated in the simulation are compared with the experimental rates in Figure 8. The chemical reaction rate and the maximum solid state diffusion rate of iron (expressed in mol/(m² s)) have been converted to mm/y equivalent corrosion rates for this comparison. No inner scale was formed

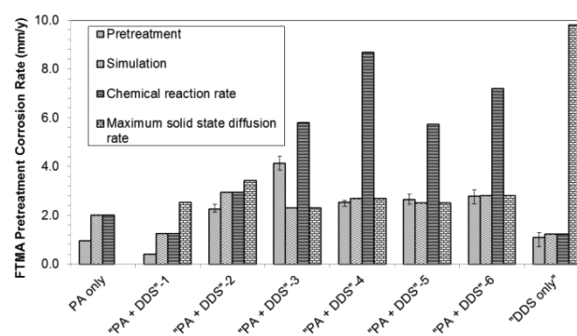


Figure 8. Model validation with pretreatment corrosion rates of A106 specimens pretreated with a series of solutions in FTMA at 343 °C.

in PA only, so the maximum solid state diffusion rate is not applicable. The simulated results fit experimental ones within a reasonable range. Corrosion was controlled by chemical reactions for DDS only and PA + DDS-1 and -2 given fast solid state diffusion rate through thin inner scales. With higher sulfur content in other solutions, the solid state diffusion of iron was deterred by thick inner scales and became the rate-determining step.

Scales formed by experimental solutions were exposed to attack by TCI only at 343 °C in the challenge experiment. As reported in our prior publication⁴⁷ and summarized in Table S2, most inner scales were thinner (even completely dissolved in case of PA + DDS-4) after the challenge experiment. Therefore, solid state diffusion was not the rate-limiting step and the challenge corrosion rate was controlled by the chemical reaction on the surface of inner scales (Figure 9).

In order to examine the model's performance at different temperatures, A106 specimens were pretreated with PA + DDS-1 and -2 in FTMA at 316 and 288 °C.⁴⁸ For the same experimental solution, lower pretreatment temperature resulted in a thinner inner scale (Table S3). As shown in Figures 10 and 11, corrosion rates were simulated within an acceptable range

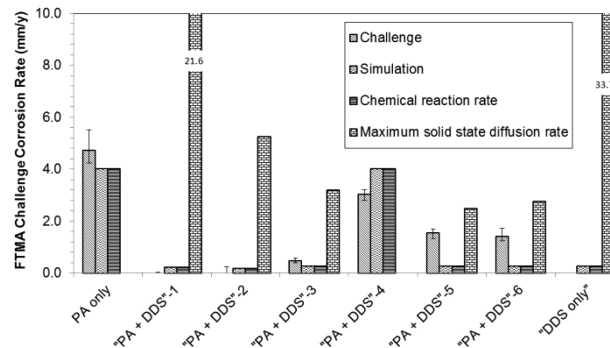


Figure 9. Model validation with challenge corrosion rates of A106 specimens pretreated with experimental solutions at 343 °C and challenged with TCI only at 343 °C.

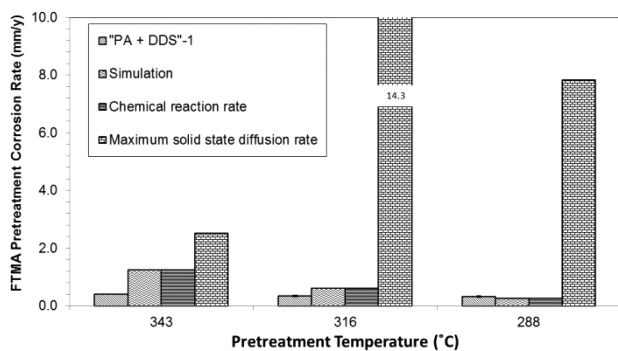


Figure 10. Model validation with pretreatment corrosion rates of A106 specimens pretreated with PA + DDS-1 in FTMA at 343, 316, or 288 °C.

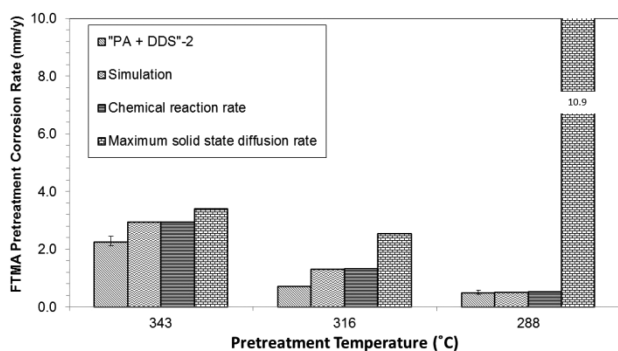


Figure 11. Model validation with pretreatment corrosion rates of A106 specimens pretreated with PA + DDS-2 in FTMA at 343, 316, or 288 °C.

of error. The thin inner scales allowed fast solid state diffusion of iron, and the chemical reaction was the rate-determining step at 316 and 288 °C.

4.5. Development toward a Predictive Model. In sections above, a model was built to simulate the sulfidation and NAC on the basis of corrosion mechanism. The proposed model and corrosion mechanism was validated with results of a series of experiments. It was found that properties of inner scales (chemical composition and thickness) are critical factors to simulate the corrosion rate. However, these properties are not available in the crude oil refineries. So the model is limited

to simulation until such time that those values can be predicted from properties that can be measured.

Some additional obstacles still exist in building a predictive model. First, kinetic constants of the dissolution rate of iron sulfide by NAP (reaction R9) have only been estimated indirectly as discussed above; exact values of activation energy and pre-exponential factor should be determined directly. The formation of magnetite by thermal decomposition of iron carboxylates (reactions R1 and R2) has been confirmed by the detection of ketones in post-test corrosion oils.⁶³ The reaction has been studied extensively in the preparation of nanoparticulate magnetite and the synthesis of ketones in concentrated solutions of model acids in relatively inert solvents. Much remains to be determined about the mechanism of magnetite formation on and within the sulfide scale including the effects of acid molecular structure and the kinetics of iron naphthenate formation and thermal decomposition.

Likewise, the mechanism governing the growth of inner scale is not fully understood. As shown in Figure 12, the inner scale thickness increased with sulfur content in pretreatment solutions PA + DDS-1, -2, and -3 but stopped growing for higher sulfur content, following the same trend of corrosion rates. In a preliminary study, A106 specimens were pretreated in PA + DDS-1 at 343 °C for up to 72 h (Figure 13). It was found that the thickness of inner scale culminated after the 48-h pretreatment and longer pretreatment did not result in a significant change of inner scale thickness. These results suggest that there may be a maximum inner scale thickness under a given experimental condition that might be related to the mechanical stress of scale growth that leads to the delamination of the outer scale.

Eventually, the effect of flow and flow turbulence will need to be factored into a predictive model. The present work with the FTMA provides a replenishment flow that simulates steady state conditions in the refinery, i.e. steel exposed to a constant concentration of reactants for a brief period and soluble corrosion product (iron naphthenates) swept away from the steel surface. Therefore, the FTMA minimizes effects of the solution chemistry without exerting any mechanical stress on the scale as it forms on the surface. Alternative testing equipment will be required to determine the effect of flow turbulence on scale formation.

Ongoing research in our group is focusing on identifying properties and their measurement that can be factors in a

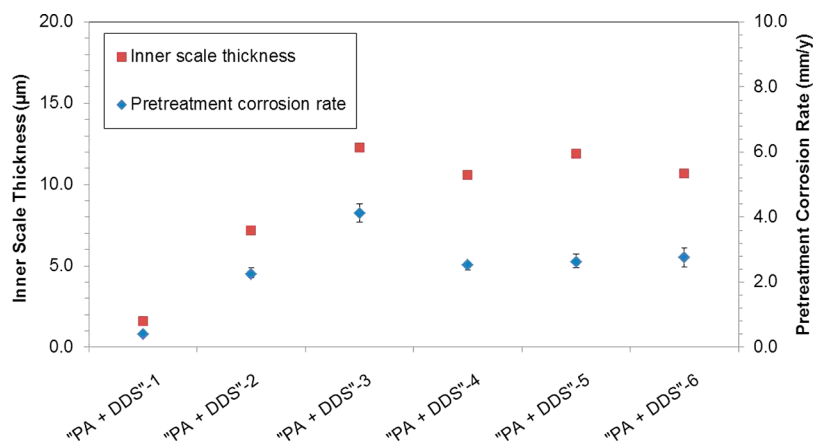


Figure 12. Inner scale thickness and pretreatment corrosion rates of A106 specimens pretreated with experimental solutions in FTMA at 343 °C for 24 h.

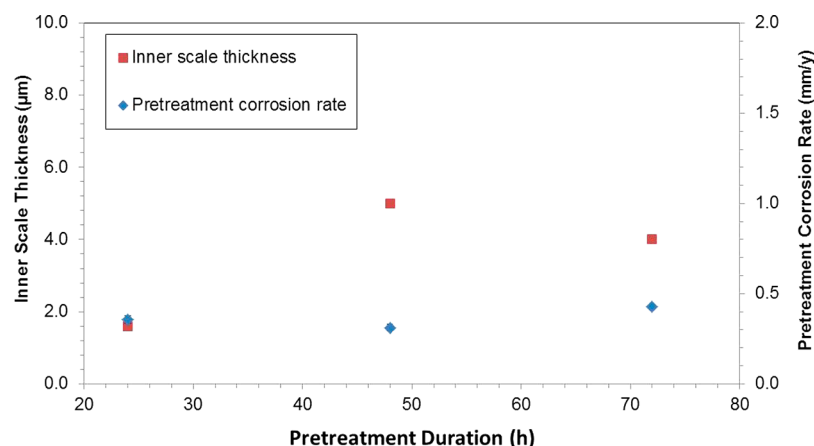


Figure 13. Inner scale thickness and pretreatment corrosion rates of A106 specimens pretreated with PA + DDS-1 in FTMA at 343 °C for 24, 48, or 72 h.

predictive model for sulfidation and NAC reactions. Compared with existing models, the predictive model will be based on the corrosion mechanism, incorporating solid state diffusion, flow dynamics, and chemical reactions.

5. CONCLUSION

High-temperature corrosion by NAP and sulfur compounds was found to be governed by solid state diffusion of iron through the inner scale and the chemical reactions on the surface of the inner scale. Both NAC and sulfidation proceeded on top of the inner scale. A mechanistic model was built on the basis of chemical reaction kinetics, solid state diffusion of iron, and flow dynamics. In addition to activation energies, values of pre-exponential terms for NAC and sulfidation were calculated. Model validation showed satisfactory agreement with experimental results. Current study laid the cornerstone for a predictive model.

■ ASSOCIATED CONTENT

Supporting Information

The Supporting Information is available free of charge on the ACS Publications website at DOI: [10.1021/acs.iecr.8b00250](https://doi.org/10.1021/acs.iecr.8b00250).

Thickness and average chemical composition of inner scales formed in FTMA pretreatment; thickness and average chemical composition of inner scales formed in FTMA pretreatment and challenge; thickness and average chemical composition of inner scales formed in FTMA pretreatment with solutions at 316 or 288 °C (PDF)

■ AUTHOR INFORMATION

Corresponding Author

*E-mail: pj221108@ohio.edu.

ORCID

Peng Jin: 0000-0002-9318-0498

Notes

The authors declare no competing financial interest.

■ ACKNOWLEDGMENTS

This work was supported by Naphthenic Acid Corrosion Joint Industry Project (NAP JIP) in the Institute for Corrosion and Multiphase Technology, Ohio University.

■ LIST OF SYMBOLS

Abbreviations

- CS = carbon steel
- DDS = *n*-dodecyl sulfide
- EDS = energy dispersive X-ray spectroscopy
- FTMA = flow through mini autoclave
- NAC = naphthenic acid corrosion
- NAP = naphthenic acid
- PA = palmitic acid
- Re = Reynolds number
- Sc = Schmidt number
- SEM = scanning electron microscope
- Sh = Sherwood number
- TCI = mixture of naphthenic acids available from TCI America

Nomenclature

- $A_{\text{NAC on FeS}}$ = pre-exponential term for naphthenic acid corrosion on troilite surface (m/s)
- $A_{\text{NAC on steel}}$ = pre-exponential term for naphthenic acid corrosion on bare steel surface (m/s)
- $A_{\text{sulfidation}}$ = pre-exponential term for sulfidation (m/s)
- $C_{0,\text{Fe}}$ = concentration of iron on the inner surface of inner scale (mol/m³)
- $C_{i,\text{Fe}}$ = concentration of iron on the outer surface of inner scale (mol/m³)
- $C_{b,\text{NAP}}$ = concentration of naphthenic acids in the bulk fluid (mol/m³)
- $C_{b,\text{sulfur}}$ = concentration of sulfur compounds in the bulk fluid (mol/m³)
- $C_{s,\text{NAP}}$ = concentration of naphthenic acids on the outer surface of inner scale (mol/m³)
- $C_{s,\text{sulfur}}$ = concentration of sulfur compounds on the outer surface of inner scale (mol/m³)
- CR_1 = pretreatment corrosion rate (mm/y)
- CR_2 = challenge corrosion rate (mm/y)
- $CR_{\text{simulation}}$ = simulated corrosion rate (mm/y)
- $D_{0,\text{C20}}$ = pre-exponential factor for self-diffusion of C20 paraffin (m²/s)
- $D_{0,\text{Fe in Fe}_3\text{O}_4}$ = pre-exponential factor for self-diffusion of iron in magnetite (m²/s)
- $D_{0,\text{Fe in FeS}}$ = pre-exponential factor for self-diffusion of iron in troilite (m²/s)
- D_{C20} = self-diffusivity of C20 paraffin (m²/s)
- D_{eff} = effective diffusivity (m²/s)

$D_{\text{Fe in Fe}_3\text{O}_4}$ = self-diffusivity of iron in magnetite (m^2/s)
 $D_{\text{Fe in FeS}}$ = self-diffusivity of iron in troilite (m^2/s)
 $\text{FeS}_{\% \text{at}}$ = atomic percent of pyrrhotite in inner scale
 J_{Fe} = flux of iron ($\text{mol}/(\text{m}^2 \text{ s})$)
 $J_{\text{Fe,max}}$ = maximum flux of iron ($\text{mol}/(\text{m}^2 \text{ s})$)
 J_{NAP} = flux of naphthenic acids from the bulk fluid toward the steel ($\text{mol}/(\text{m}^2 \text{ s})$)
 J_{S} = flux of sulfur compounds from the bulk fluid toward the steel ($\text{mol}/(\text{m}^2 \text{ s})$)
 ΔH_{C20} = activation energy for self-diffusion of C20 paraffin (kJ/mol)
 $\Delta H_{\text{Fe in Fe}_3\text{O}_4}$ = activation energy for self-diffusion of iron in magnetite (kJ/mol)
 $\Delta H_{\text{Fe in FeS}}$ = activation energy for self-diffusion of iron in troilite (kJ/mol)
 $\Delta H_{\text{NAC on FeS}}$ = activation energy for naphthenic acid corrosion on troilite surface (kJ/mol)
 $\Delta H_{\text{NAC on steel}}$ = activation energy for naphthenic acid corrosion on bare steel surface (kJ/mol)
 $\Delta H_{\text{sulfidation}}$ = activation energy for sulfidation (kJ/mol)
 k = mass transfer coefficient (m/s)
 l = length of specimen (m)
 $MW_{\text{Fe}_3\text{O}_4}$ = molecular weight of magnetite (kg/mol)
 MW_{FeS} = molecular weight of pyrrhotite (kg/mol)
 R = gas constant ($\text{J}/\text{K}/\text{mol}$)
 S = area of specimen (m^2)
 $r_{\text{NAC on steel}}$ = rate of naphthenic acid corrosion on bare steel surface ($\text{mol}/(\text{m}^2 \text{ s})$)
 $r_{\text{NAC on FeS}}$ = rate of naphthenic acid corrosion on troilite surface ($\text{mol}/(\text{m}^2 \text{ s})$)
 V_{FeS} = volume fraction of troilite
 V = average flow velocity (m/s)
 ΔW_1 = weight loss in pretreatment step (kg)
 ΔW_2 = weight loss in challenge step (kg)
 t = duration of experiment (s)
 T = absolute temperature (K)
 δ = thickness of inner scale (m)
 $\Delta \delta$ = thickness change of inner scale (m)
 μ = dynamic viscosity of C20 paraffin ($\text{kg}/\text{m}/\text{s}$)
 ρ_{C20} = density of C20 paraffin (kg/m^3)
 ρ_{FeS} = density of troilite (kg/m^3)
 $\rho_{\text{Fe}_3\text{O}_4}$ = density of magnetite (kg/m^3)
 ρ_{steel} = density of A106 carbon steel (kg/m^3)

REFERENCES

- (1) Kapusta, S. D.; Ooms, A.; Smith, A.; Fort, W. C. Safe Processing of Acid Crudes. *CORROSION/2004*, New Orleans, Louisiana, USA, March 28–April 1, 2004; Paper No. 4637.
- (2) Derungs, W. A. Naphthenic Acid Corrosion – An Old Enemy of the Petroleum Industry. *Corrosion* **1956**, *12*, 41.
- (3) Kane, R. D.; Cayard, M. S. Understanding Critical Factors that Influence Refinery Crude Corrosiveness. *Mater. Perform.* **1999**, *7*, 48.
- (4) Llopis, J.; Gamboa, J. M.; Arizmendi, L.; Gomez-Minana, J. A. Surface Reactions of Iron with Hydrocarbon Solutions of Organic Sulphides. *Corros. Sci.* **1964**, *4*, 27.
- (5) Qu, D. R.; Zheng, Y. G.; Jing, H. M.; Yao, Z. M.; Ke, W. High Temperature Naphthenic Acid Corrosion and Sulphidic Corrosion of Q235 and 5Cr0.5Mo Steels in Synthetic Refining Media. *Corros. Sci.* **2006**, *48*, 1960.
- (6) Lobodin, V. V.; Robbins, W. K.; Lu, J.; Rodgers, R. P. Separation and Characterization of Reactive and Non-Reactive Sulfur in Petroleum and Its Fractions. *Energy Fuels* **2015**, *29*, 6177.
- (7) Hsu, C.; Dechert, G.; Robbins, W.; Fukuda, E. Naphthenic Acids in Crude Oils Characterized by Mass Spectrometry. *Energy Fuels* **2000**, *14*, 217.
- (8) Qian, K.; Robbins, W.; Hughey, C.; Cooper, H.; Rodgers, R.; Marshall, A. Resolution and Identification of Elemental Compositions for More Than 3000 Crude Acids in Heavy Petroleum by Negative-ion Microelectrospray High-field Fourier Transform Ion Cyclotron Resonance Mass Spectrometry. *Energy Fuels* **2001**, *15*, 1505.
- (9) Headley, J. V.; McMartin, D. W. A Review of the Occurrence and Fate of Naphthenic Acids in Aquatic Environments. *J. Environ. Sci. Health, Part A: Toxic/Hazard. Subst. Environ. Eng.* **2004**, *39*, 1989.
- (10) Tomczyk, N. A.; Winans, R. E.; Shinn, J. H.; Robinson, R. C. On the Nature and Origin of Acidic Species in Petroleum. 1. Detailed Acid Type Distribution in a California Crude Oil. *Energy Fuels* **2001**, *15*, 1498.
- (11) Hughey, C. A.; Rodgers, R. P.; Marshall, A. G.; Qian, K.; Robbins, W. K. Identification of Acidic NSO Compounds in Crude Oils of Different Geochemical Origins by Negative Ion Electro spray Fourier Transform Ion Cyclotron Resonance Mass Spectrometry. *Org. Geochem.* **2002**, *33*, 743.
- (12) Patrick, B. N.; Chakravarti, R.; Devine, T. M. Dynamic Measurements of Corrosion Rates at High Temperatures in High Electrical Resistivity Media. *Corros. Sci.* **2015**, *94*, 99.
- (13) Tebbal, S.; Podlecki, R.; Sudhakar, C.; Schutt, H. U. Analysis and Corrosivity Testing of Eight Crude Oils. *CORROSION/2004*, New Orleans, Louisiana, USA, March 28–April 1, 2004; Paper No. 4636.
- (14) Yoon, Y.; Kosacki, I.; Srinivasan, S. Naphthenic Acid and Sulfur Containing Crude Oil Corrosion: A Comparative Review. *CORROSION/2016*, Vancouver, British Columbia, Canada, March 6–10, 2016; Paper No. 2016-7598.
- (15) Yap, K.; Srinivasan, S. Predict-Crude: Quantifying Naphthenic Acid Corrosion in Refineries. *5th Annual AIChE Midwest Regional Conference*, Chicago, Illinois, USA, January 31–February 1, 2013.
- (16) Jin, P.; Bota, G.; Robbins, W.; Nescic, S. Analysis of Oxide Scales Formed in the Naphthenic Acid Corrosion of Carbon Steel. *Energy Fuels* **2016**, *30*, 6853.
- (17) Jin, P.; Nescic, S.; Wolf, H. A. Analysis of Corrosion Scales Formed on Steel at High Temperatures in Hydrocarbons Containing Model Naphthenic Acids and Sulfur Compounds. *Surf. Interface Anal.* **2015**, *47*, 454.
- (18) Jin, P.; Robbins, W.; Bota, G.; Nescic, S. Characterization of Magnetite Scale Formed in Naphthenic Acid Corrosion. *JOM* **2017**, *69*, 217.
- (19) Jin, P.; Nescic, S. Mechanism of Magnetite Formation in High Temperature Naphthenic Acid Corrosion by Crude Oil Fractions. *Corros. Sci.* **2017**, *115*, 93.
- (20) Wolf, H. A.; Cao, F.; Blum, S. C.; Schilowitz, A. M.; Ling, S.; McLAUGHLIN, J. E.; Nescic, S.; Jin, P.; Gheorghe, B. O. Method for Identifying Layers Providing Corrosion Protection in Crude Oil Fractions. U.S. Patent 9,140,640, September 22, 2015.
- (21) Squibb, E. R. Improvement in the Manufacture of Acetone. *J. Am. Chem. Soc.* **1895**, *17*, 187.
- (22) Renz, M. Ketonization of Carboxylic Acids by Decarboxylation: Mechanism and Scope. *Eur. J. Org. Chem.* **2005**, *6*, 979.
- (23) Jin, P.; Robbins, W.; Bota, G. Mechanism of Magnetite Formation in High Temperature Corrosion by Model Naphthenic Acids. *Corros. Sci.* **2016**, *111*, 822.
- (24) Baaziz, W.; Pichon, B. P.; Fleutot, S.; Liu, Y.; Lefevre, C.; Greneche, J. M.; Toumi, M.; Mhiri, T.; Begin-Colin, S. Magnetic Iron Oxide Nanoparticles: Reproducible Tuning of the Size and Nanosized-dependent Composition, Defects, and Spin Canting. *J. Phys. Chem. C* **2014**, *118*, 3795.
- (25) Stolen, S.; Gloeckner, R.; Gronvold, F. Nearly Stoichiometric Iron Monoxide Formed as a Metastable Intermediate in a Two-Stage Disproportionation of Quenched Wüstite. Thermodynamic and Kinetic Aspects. *Thermochim. Acta* **1995**, *256*, 91.

- (26) Patrick, B. N. Understanding Naphthenic Acid Corrosion in Refinery Settings. Ph.D. Dissertation, University of California, Berkeley, California, USA, 2015.
- (27) Slavcheva, E.; Shone, B.; Turnbull, A. Review of Naphthenic Acid Corrosion in Oil Refining. *Br. Corros. J.* **1999**, *34*, 125.
- (28) Li, W.; Landon, J.; Irvin, B.; Zheng, L.; Ruh, K.; Kong, L.; Pelgen, J.; Link, D.; Figueroa, J. D.; Thompson, J.; Nikolic, H.; Liu, K. Use of Carbon Steel for Construction of Post-combustion CO₂ Capture Facilities: A Pilot-scale Corrosion Study. *Ind. Eng. Chem. Res.* **2017**, *56*, 4792.
- (29) Li, W.; Brown, B.; Young, D.; Nešić, S. Investigation of Pseudo-passivation of Mild Steel in CO₂ Corrosion. *Corrosion* **2014**, *70*, 294.
- (30) Jia, R.; Yang, D.; Al-Mahamedh, H. H.; Gu, T. Electrochemical testing of biocide enhancement by a mixture of D-amino acids for the prevention of a corrosive biofilm consortium on carbon steel. *Ind. Eng. Chem. Res.* **2017**, *56*, 7640.
- (31) Han, J.; Young, D.; Colijn, H.; Tripathi, A.; Nešić, S. Chemistry and Structure of the Passive Film on Mild Steel in CO₂ Corrosion Environments. *Ind. Eng. Chem. Res.* **2009**, *48*, 6296.
- (32) Sun, W.; Nešić, S.; Young, D.; Woollam, R. C. Equilibrium Expressions Related to the Solubility of the Sour Corrosion Product Mackinawite. *Ind. Eng. Chem. Res.* **2008**, *47*, 1738.
- (33) Zhao, W.; Zou, Y.; Matsuda, K.; Zou, Z. Characterization of the Effect of Hydrogen Sulfide on the Corrosion of X80 Pipeline Steel in Saline Solution. *Corros. Sci.* **2016**, *102*, 455.
- (34) Gao, S.; Jin, P.; Brown, B.; Young, D.; Nestic, S.; Singer, M. Corrosion Behavior of Mild Steel in Sour Environments at Elevated Temperatures. *Corrosion* **2017**, *73*, 915.
- (35) Mehrer, H. *Diffusion in Solids: Fundamentals, Methods, Materials, Diffusion-controlled Processes*; Springer: Münster, Germany, 2007.
- (36) Fryt, E. M.; Smeltzer, W. W.; Kirkaldy, J. S. Chemical Diffusion and Point Defect Properties of Iron Sulfide (Fe_{1-δ}S) at Temperatures 600°–1000°C. *J. Electrochem. Soc.* **1979**, *126*, 673.
- (37) Sterten, A. Nonstoichiometry and Diffusivities in Iron Monosulfide at Elevated Temperatures. *Corros. Sci.* **1974**, *14*, 377.
- (38) Hobbins, R. Self-Diffusion of Iron in Single Crystals of Ferrous Sulfide and Magnetically Saturated Iron. Ph.D. Dissertation, University of Delaware, Delaware, Newark, USA, 1969.
- (39) Condit, R.; Hobbins, R.; Birchenall, C. Self-Diffusion of Iron and Sulfur in Ferrous Sulfide. *Oxid. Met.* **1974**, *8*, 409.
- (40) Marusak, L. A.; Mulay, L. N. Polyttypism in the Cation-deficient Iron Sulfide, Fe₉S₁₀, and the Magnetokinetics of the Diffusion Process at Temperatures about the Antiferro- to Ferrimagnetic (λ) Phase Transition. *Phys. Rev. B: Condens. Matter Mater. Phys.* **1980**, *21*, 238.
- (41) Danielewski, M.; Mrowec, S.; Stołosa, A. Sulfidation of Iron at High Temperatures and Diffusion Kinetics in Ferrous Sulfide. *Oxid. Met.* **1982**, *17*, 77.
- (42) William Herbert, F. W.; Krishnamoorthy, A.; Rands, L.; Van Vliet, K. J.; Yildiz, B. Magnetic Diffusion Anomaly at the Néel Temperature of Pyrrhotite, Fe_{1-x}S. *Phys. Chem. Chem. Phys.* **2015**, *17*, 11036.
- (43) Himmel, L.; Mehl, R. F.; Birchenall, C. E. Self-diffusion of Iron in Iron Oxides and the Wagner Theory of Oxidation. *JOM* **1953**, *197*, 827.
- (44) Herbert, F. W.; Krishnamoorthy, A.; Yildiz, B.; Van Vliet, K. J. Diffusion-limited Kinetics of the Antiferromagnetic to Ferrimagnetic λ -Transition in Fe_{1-x}S. *Appl. Phys. Lett.* **2015**, *106*, 092402.
- (45) Pareek, V. K.; Ramanarayanan, T. A.; Mumford, J. D.; Ozekcin, A.; Scanlon, J. C. The Role of Morphology and Structure in the Kinetic Evolution of Iron-sulfide Films on Fe-base Alloys. *Oxid. Met.* **1994**, *41*, 323.
- (46) Pareek, V. K.; Ramanarayanan, T. A.; Mumford, J. D. Kinetics of Sulfur Transfer from H₂S to Fe_{1-x}S. *Catal. Lett.* **1997**, *46*, 223.
- (47) Jin, P.; Robbins, W.; Bota, G. Effect of sulfur compounds on formation of protective scales in naphthenic acid corrosion in non-turbulent flow. *Corros. Sci.* **2018**, *131*, 223.
- (48) Jin, P.; Robbins, W.; Bota, G. Effect of temperature on scale formation in high-temperature corrosion by model naphthenic acids and sulfur compounds under replenishing conditions. *Energy Fuels* **2017**, *31*, 10222.
- (49) Barney, M. M.; Embaid, B. P.; Nissan, A. Identifying phases in protective scale formed during high temperature corrosion. *Corros. Sci.* **2017**, *127*, 21.
- (50) Hallström, S.; Höglund, L.; Ågren, J. Modeling of iron diffusion in the iron oxides magnetite and hematite with variable stoichiometry. *Acta Mater.* **2011**, *59*, 53.
- (51) Bota, G. M.; Corrosion of Steel at High Temperature in Naphthenic Acid and Sulfur Containing Crude Oil Fractions. Ph.D. dissertation, Ohio University, Athens, OH, 2010.
- (52) Turnbull, A.; Slavcheva, E.; Shone, B. Factors Controlling Naphthenic Acid Corrosion. *Corrosion* **1998**, *54*, 922.
- (53) *Annual Book of ASTM Standards*; West Conshohocken, PA, 2011; Vol. 03.02.
- (54) Clarke, S. G. The Use of Inhibitors (with Special Reference to Antimony) in the Selective Removal of Metallic Coatings and Rust. *Trans. Electrochem. Soc.* **1936**, *69*, 131.
- (55) Yu, J.; Jiang, L.; Gan, F. High Temperature Naphthenic Acid Corrosion of Steel in High TAN Refining Media. *Anti-Corros. Methods Mater.* **2008**, *55*, 257.
- (56) Gutzeit, J. Naphthenic Acid Corrosion in Oil Refineries. *Mater. Perform.* **1977**, *16*, 24.
- (57) Herbert, F. W.; Mechanisms governing the growth, reactivity and stability of iron sulfides. Ph.D. dissertation, Massachusetts Institute of Technology, Cambridge, Massachusetts, USA, 2015.
- (58) Douglass, D. C.; McCall, D. W. Diffusion in Paraffin Hydrocarbons. *J. Phys. Chem.* **1958**, *62*, 1102.
- (59) Ertl, H.; Dullien, F. A. L. Self-diffusion and Viscosity of Some Liquids as a Function of Temperature. *AIChE J.* **1973**, *19*, 1215.
- (60) Bachl, F.; Lüdemann, H. D. Pressure and Temperature Dependence of Self-diffusion in Liquid Linear Hydrocarbons. *Z. Naturforsch., A: Phys. Sci.* **1986**, *41*, 963.
- (61) Permutt, G. Absolute Viscosity of the n-Paraffin Liquids. Master of Science thesis, New Jersey Institute of Technology, Newark, New Jersey, USA, 1960.
- (62) Van den Berg, G. B.; Racz, I. G.; Smolders, C. A. Mass Transfer Coefficients in Cross-flow Ultrafiltration. *J. Membr. Sci.* **1989**, *47*, 25.
- (63) Krajewski, L. C.; Lobodin, V. V.; Robbins, W. K.; Jin, P.; Bota, G.; Marshall, A. G.; Rodgers, R. P. Method for isolation and detection of ketones formed from high-temperature naphthenic acid corrosion. *Energy Fuels* **2017**, *31*, 10674.